S1. Optimization process of the synthesis of composite bubbles

The synthesis protocol reported in the main article is a modification of the protocol originally reported in ref (Vassalini et al., 2020), which required 80 mg sodium alginate and 20 mg sodium citrate and a 0.2 M $CaCl_2$ solution for crosslinking. One of the problems encountered during the preparation of our composite systems was the fact that Fe_3O_4 particles (even at low quantity) tend to settle down when added to sodium alginate solution, resulting in the preparation of non-homogeneous hydrogel bubbles characterized by poor magnetic properties. In order to solve this problem, the amounts of sodium alginate ad sodium citrate were increased, so that it was possible to obtain a solution characterized by a higher viscosity. After several tests for parameter optimization, reported in Table S1, the amount of 200 mg sodium alginate and 50 mg sodium citrate were selected, since the solution became sticky enough to suspend Fe_3O_4 particles. The synthesized bubbles in these conditions could effectively respond to the application of an external magnetic field (sample #5). However, as the concentration of sodium alginate increased, the molarity of crosslinker $CaCl_2$ at 0.2M was insufficient and the resulted bubbles were not completely homogeneous, and they have white stains on their surface. These white stains disappeared when the molarity of the crosslinking solution was increased from 0.2M to 0.6M (sample #6).

Although sodium citrate is known as a strong Cr^{3+} chelating agent (Kantar et al., 2015), complexes between Cr^{3+} and citrate are also prone to photo-oxidation and regeneration of Cr^{6+} could occur (Dai et al., 2010). Moreover, sodium citrate forms a complex with Ca^{2+}, soften the hydrogels and speeds up the degradation process (Wen et al., 2019). For these reasons, we decided to remove sodium citrate from the recipe of the synthesis of the composite bubbles, as visible in samples #7-9. This modification could have impact also on the adsorbability of the hydrogel bubbles, as a higher amount of free Ca^{2+} ions is available for electrostatic interaction with CrO_4^{2-} and $Cr_2O_7^{2-}$, maximizing Cr capture. The optimized synthesis protocol is that reported in Table S1-sample #9.

<table>
<tr><th>sample No.</th><th>Sodium alginate</th><th>Sodium citrate</th><th>Fe_3O_4</th><th>AC</th><th>VitC</th><th>Molarity of $CaCl_2$</th><th>Note</th></tr>
<tr><td>#1</td><td rowspan="4">80 mg</td><td rowspan="4">20 mg</td><td>20 mg</td><td>50 mg</td><td rowspan="6">-</td><td rowspan="5">0.2 M</td><td rowspan="4">Poor magnetic attraction</td></tr>
<tr><td>#2</td><td>20 mg</td><td rowspan="6">70 mg</td></tr>
<tr><td>#3</td><td>100 mg</td></tr>
<tr><td>#4</td><td>200 mg</td></tr>
<tr><td>#5</td><td rowspan="4">200 mg</td><td rowspan="2">50 mg</td><td rowspan="4">100 mg</td><td>White stain on bubbles</td></tr>
<tr><td>#6</td><td rowspan="3">0.6 M</td><td>-</td></tr>
<tr><td>#7</td><td rowspan="2">-</td><td>-</td></tr>
<tr><td>#8</td><td>50 mg</td><td>-</td></tr>
<tr><td>#9</td><td>100 mg</td><td>Optimised bubbles</td></tr>
</table>

Table S1. Parameters optimization for the hydrogel bubbles synthesis

S2. Chemical composition of mineral water used for the preparation of true-to-life wastewater samples

Ca^{2+} [mg/L]	Mg^{2+} [mg/L]	K^+ [mg/L]	HCO_3^- [mg/L]	SiO_2 [mg/L]	Cl^- [mg/L]	SO_4^{2-} [mg/L]	NO^-_3 [mg/L]	F^- [mg/L]
82.4	10.2	0.94	232	9.3	3.2	4.3	2.2	0.23

Table S2. Concentration of chemical species in mineral water used for the preparation of true-to-life wastewater samples

S3. UV-vis spectroscopic quantification of Cr(VI) in wastewater

For the analysis of concentrated samples, quantification of Cr^{6+} was directly derived from the absorption peak at 350 – 374 nm.

As example, the UV-vis spectrum obtained for a Cr(VI) solution in ultrapure water with a concentration equal to 20 mg/L is reported in **Figure S3a,** while the calibration curve for the concentration range 1-20 mg/L is reported in **Figure S3b**. It was obtained by reading the absorbance values at 350 nm.

When the Cr(VI) concentration was low and the solution was colorless, the Cr^{6+} concentration was obtained from an indirect measurement, using diphenylcarbazide (DPC) as complexing agent and marker (USEPA; method 7196A). In fact, Cr(VI) forms a colored complex when combined with DPC, which can be detected by UV-Vis spectrophotometry with an absorbance edge at 540 nm, as shown in **Figure S3c** in the case of a Cr(VI) solution with a concentration of 0.8 mg/L. The calibration curve in the concentration range 0.025-0.8 mg/L is reported in **Figure S3d**.

When solutions were prepared in mineral water, the absorption spectrum was a little bit modified as visible in **Figure S3e**: the maximum of the absorbance was redshifted (maximum at 373 nm) and the intensity was slightly enhanced. These modifications are in line with what reported in literature, considering variation of solution pH (i.e. for a solution of Cr(VI) 20 mg/L pH passes from 6.3 for ultrapure water to 7.9 for mineral water). The calibration curve for the concentration range 1-20 mg/L in the case of mineral water is reported in **Figure S3f**. It was obtained by reading the absorbance values at 373 nm.

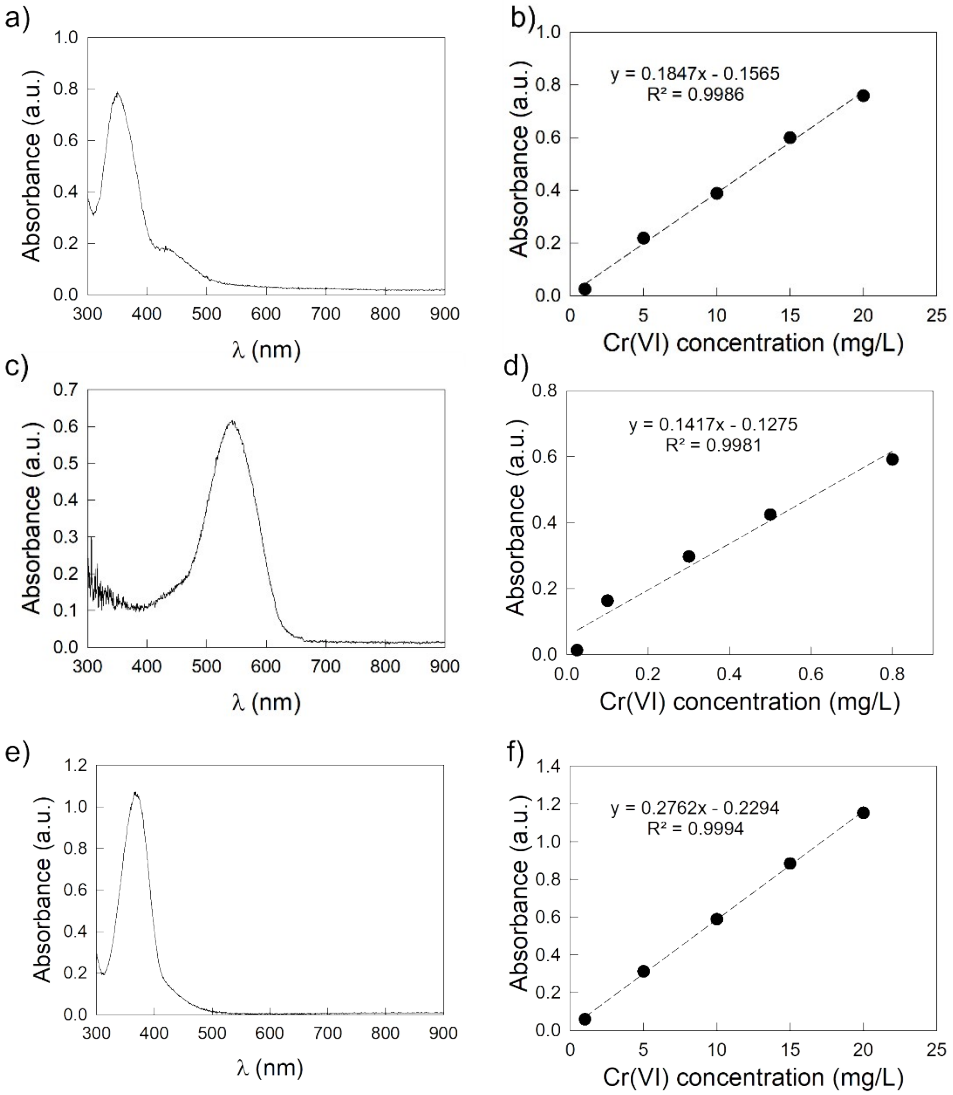

Fig S3. a) UV-vis spectrum of a 20 mg/L Cr^{6+} solution in ultrapure water; b) calibration curve for direct spectroscopic Cr^{6+} quantification (1-20 mg/L) in ultrapure water; c) UV-vis spectrum of a 0.8 mg/L Cr^{6+} solution, by indirect measurement with DPC; d) calibration curve for indirect UV-vis Cr^{6+} quantification with DPC (0.025-0.8 mg/L); e) UV-vis spectrum of a 20 mg/L Cr^{6+} solution in mineral water; f) calibration curve for direct spectroscopic Cr^{6+} quantification (1-20 mg/L) in mineral water.

S4. Individuation of the best kinetic model for the fitting of adsorption data

From the adsorption data and through the formula

$$q_t = (C_0 - C_t) \times (V/m) \quad (1)$$

where C_0 corresponds to the starting Cr^{6+} concentration (mg/L), C_t is the Cr^{6+} concentration at a particular sampling time (mg/L), V is the volume of Cr^{6+} wastewater solution (L) and m is the weight of dried adsorbent (g), it was possible to calculate the adsorption capacity of the Fe_3O_4/AC/VitC bubbles at any time (q_t, mg/g) and the equilibrium adsorption capacity (q_e, mg/g).

In order to individuate the best kinetic model for the fitting of the adsorption data, the obtained values of q_t and q_e were used for the creation of the graphs corresponding to the different kinetic models, as reported in **Figure S4**.

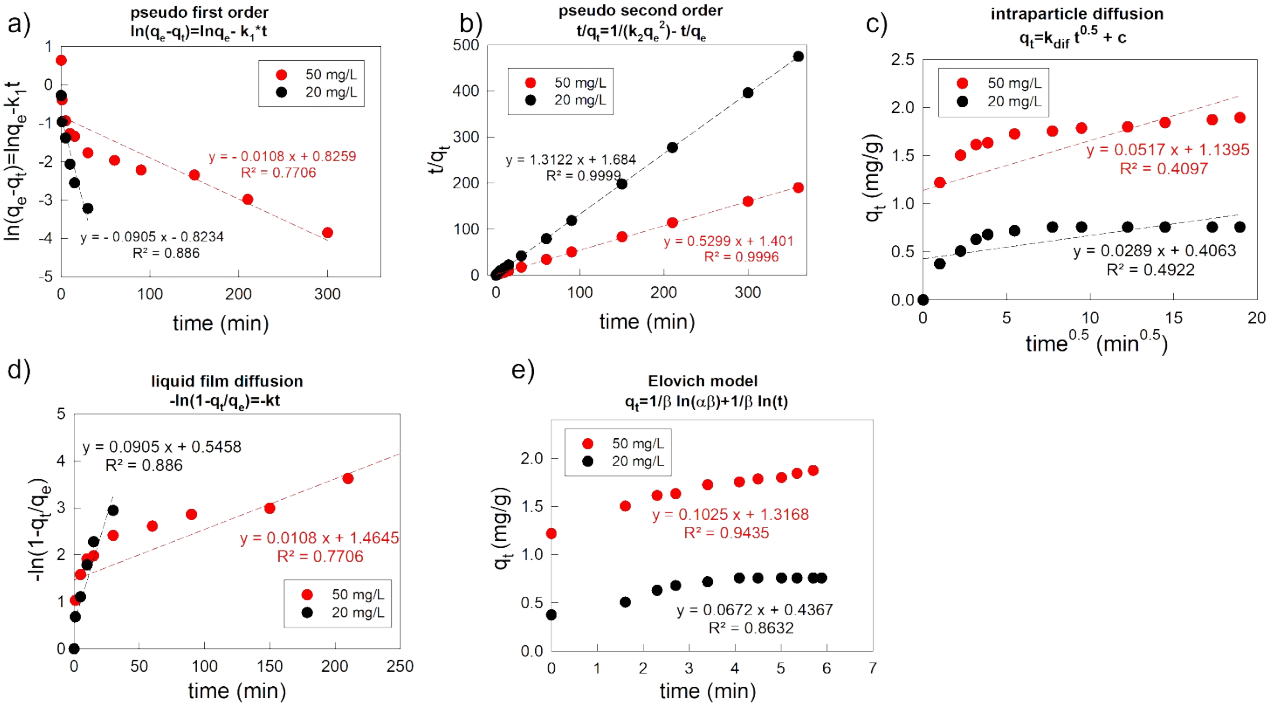

Figure S4. Different kinetic models for the fitting of the experimental adsorption data.

As visible from the Figure S6, the highest correlation coefficient value ($R^2 > 0.99$) was obtained in the case of the pseudo second order model, whose linear plot is reported also in Figure 2c of the main text. According to equation 2

$$\frac{t}{q_t} = \frac{1}{k_2 q_e^2} + \frac{t}{q_e} \quad (2)$$

it was possible to calculate the rate constant of pseudo second order adsorption process (k_2) and the value of q_e, respectively from the slope and intercept of the linear plot of t/q_t versus time (t).

S5. Optical characterization of the Fe_3O_4 powder

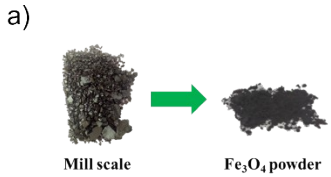

b)

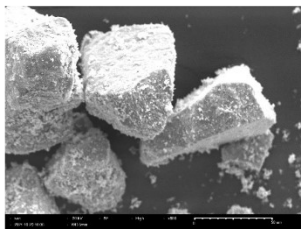

	Oxygen	Aluminum	Silicon	Iron	Gold
Normalized mass concentration [%]	11.93	0.67	0.17	77.56	9.68
Standard deviation	± 2.22	± 0.11	± 0.03	± 2.03	± 0.93

Figure S5. a) Optical picture of the mill scale and the derived Fe_3O_4 powder; b) SEM image and EDX analysis of the Fe_3O_4 powder

S6. Video showing the magnetic attraction between the composite Fe_3O_4/AC/VitC-alginate bubbles and a common magnet.

This video has been uploaded as Supporting Information. The video is available at the following link:

https://drive.google.com/drive/folders/1ZASJUR_DVDG7h1Prorz9eOqvqAahwtTM?usp=share_link

S7. Investigation of the thermal stability of the composite Fe_3O_4/AC/VitC-alginate bubbles

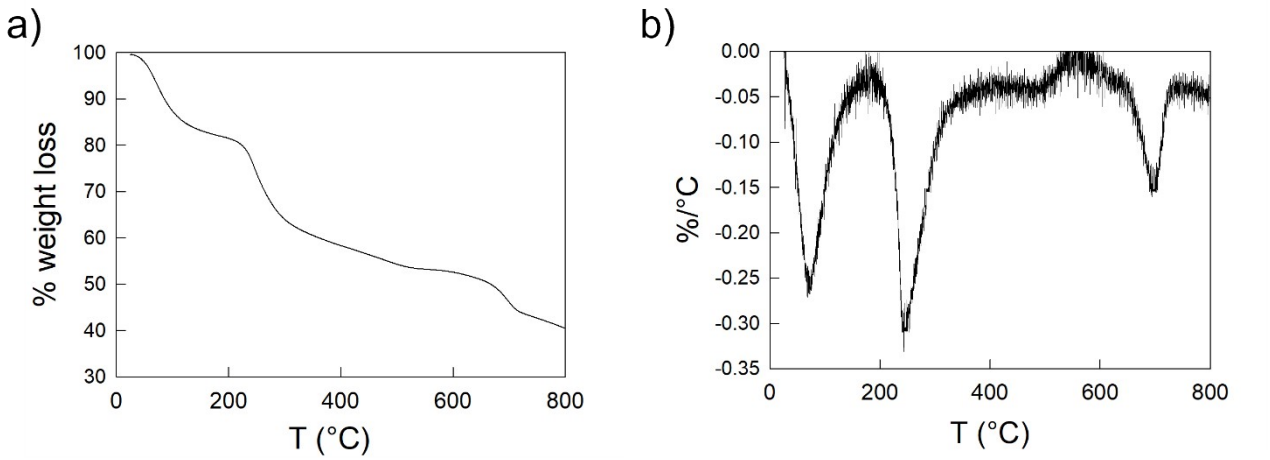

Figure S7. a) TGA curve of Fe_3O_4/AC/VitC-alginate bubbles; b) DTG curve of Fe_3O_4/AC/VitC-alginate bubbles

S8. ATR-FTIR characterization of alginate and Fe_3O_4/AC/VitC-alginate bubbles

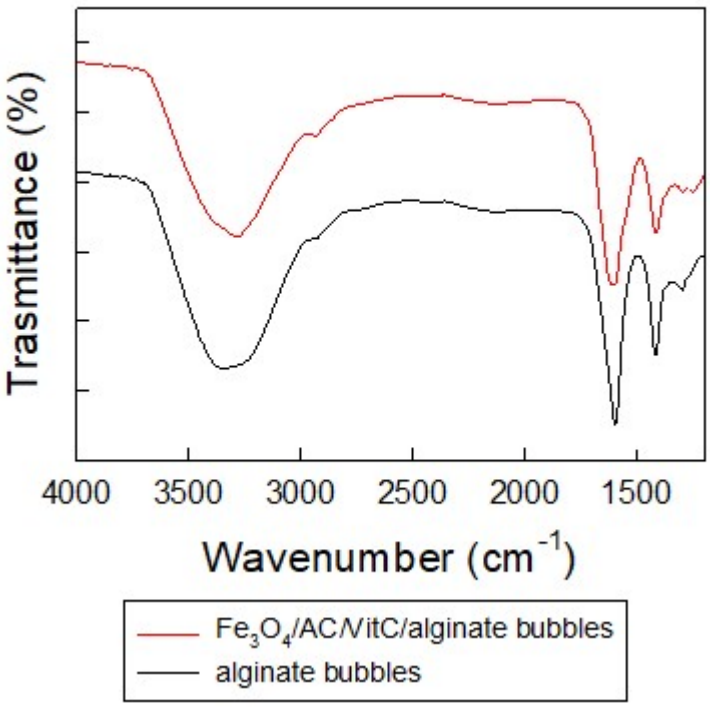

Figure S8. ATR-FTIR spectrum of Fe_3O_4/AC/VitC-alginate bubbles and bubbles made of alginate only.

S9. Comparison between the removal performances of the Fe_3O_4/AC/VitC-alginate bubbles and literature

Comparison with literature (20 mg/L)

Adsorbent	**Removal efficiency [%]**	**pH**	**Adsorption time [min]**	**Reference**
Reduced Graphene Oxide-Based Gum Tragacanth (GT-cl-poly(DMA)/RGO) Hydrogel Nanocomposite	81.5%	3.5	570	(Sharma et al., 2020)
Hydrogel-supported sulfidated nano zero-valent iron (S-nZVI@H)	100%	6.0	60	(Jing et al., 2021)
Cu-Fe embedded cross-linked 3D hydrogel	97.1%	5.0	300	(Wang et al., 2021)
Fe_3O_4/AC/VitC- alginate hydrogel	100%	6.3 (no pH buffer)	60	This work

Comparison with literature (50 mg/L)

Adsorbent	**Removal efficiency [%]**	**pH**	**Adsorption time [min]**	**Reference**
Novel three-dimensional chitosan-carbon nanotube–PVA nanocomposite Hydrogel (Cs/MWCNT/PVA)	~80%	1.5	240	(Eldeeb et al., 2020)
Crosslinked hydrogels of polyethylenimine and graphene oxide (GO/PEI-NCH)	97%	2.0	~60	(Mittal et al., 2021)
Biochar-embedding iron-alginate microspheres derived from bagasse	99.4% at 8 hr and 100% at 24 hr	2.0	480 – 1440 (8- 24 hr)	(Wang et al., 2022)
Fe_3O_4/AC/VitC- alginate hydrogel	100%	5.5 (no pH buffer)	300	This work

S10. Cr(VI) removal by mill-scale derived Fe_3O_4 powder

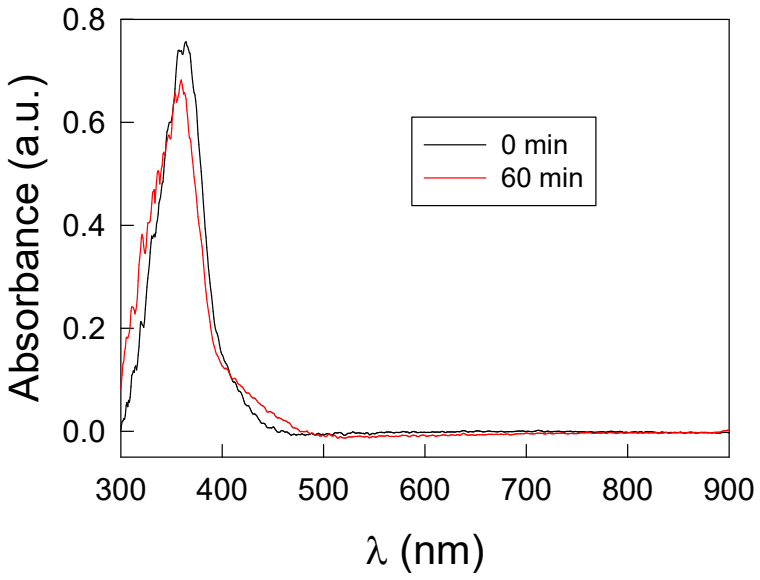

Figure S10. UV-vis spectrum of a 20 mg/L Cr^{6+} solution in ultrapure water before (black line) and after (red line) the interaction with mill-scale derived Fe_3O_4 microparticles powder for 60 minutes.

References

Dai, R., Yu, C., Liu, J., Lan, Y., Deng, B., 2010. Photo-Oxidation of Cr(III)−Citrate Complexes Forms Harmful Cr(VI). Environ. Sci. Technol. 44, 6959–6964. https://doi.org/10.1021/es100902y

Guo, X., Liu, A., Lu, J., Niu, X., Jiang, M., Ma, Y., Liu, X., Li, M., 2020. Adsorption Mechanism of Hexavalent Chromium on Biochar: Kinetic, Thermodynamic, and Characterization Studies. ACS Omega 5, 27323–27331. https://doi.org/10.1021/acsomega.0c03652

Gupta, V.K., Agarwal, S., Saleh, T.A., 2011. Chromium removal by combining the magnetic properties of iron oxide with adsorption properties of carbon nanotubes. Water Research 45, 2207–2212. https://doi.org/10.1016/j.watres.2011.01.012

Jing, Q., You, W., Tong, L., Xiao, W., Kang, S., Ren, Z., 2021. Response surface design for removal of Cr(VI) by hydrogel-supported sulfidated nano zero-valent iron (S-nZVI@H). Water Science and Technology 84, 1190–1205. https://doi.org/10.2166/wst.2021.312

Kantar, C., Ari, C., Keskin, S., 2015. Comparison of different chelating agents to enhance reductive Cr(VI) removal by pyrite treatment procedure. Water Research 76, 66–75. https://doi.org/10.1016/j.watres.2015.02.058

Sharma, B., Thakur, S., Trache, D., Yazdani Nezhad, H., Thakur, V.K., 2020. Microwave-Assisted Rapid Synthesis of Reduced Graphene Oxide-Based Gum Tragacanth Hydrogel Nanocomposite for Heavy Metal Ions Adsorption. Nanomaterials 10, 1616. https://doi.org/10.3390/nano10081616

Vassalini, I., Gjipalaj, J., Crespi, S., Gianoncelli, A., Mella, M., Ferroni, M., Alessandri, I., 2020. Alginate-Derived Active Blend Enhances Adsorption and Photocatalytic Removal of Organic Pollutants in Water. Advanced Sustainable Systems 4, 1900112. https://doi.org/10.1002/adsu.201900112

Wang, H., Zhao, X., Yang, X., Sun, S., Wang, W., Mao, Y., Song, Z., 2022. Biochar-embedding iron-alginate microspheres derived from bagasse by one-step microwave pyrolysis/activation for enhanced Cr(VI) removal. Frontiers in Energy Research 10.

Wang, Y., Lin, N., Gong, Y., Wang, R., Zhang, X., 2021. Cu–Fe embedded cross-linked 3D hydrogel for enhanced reductive removal of Cr(VI): Characterization, performance, and mechanisms. Chemosphere 280, 130663. https://doi.org/10.1016/j.chemosphere.2021.130663

Wen, K., Li, Y., Huang, W., Armwood, C., Amini, F., Li, L., 2019. Mechanical behaviors of hydrogel-impregnated sand. Construction and Building Materials 207, 174–180. https://doi.org/10.1016/j.conbuildmat.2019.02.141

Xu, X.-R., Li, H.-B., Li, X.-Y., Gu, J.-D., 2004. Reduction of hexavalent chromium by ascorbic acid in aqueous solutions. Chemosphere 57, 609–613. https://doi.org/10.1016/j.chemosphere.2004.07.031